Selective Delivery Of Photothermal Nanoparticles To Tumors Using Mesenchymal Stem Cells As Trojan-Horses.

M. Mar Encabo-Berzosa [a,b,c], Marina Gimeno[d], Lluís Luján[d], Leyre Gómez [a,b], Victor Sebastian[a,b], Miguel Quintanilla[e], Manuel Arruebo [a,b,§], Jesús Santamaría [a,b], Pilar Martín-Duque [c,f,g§]

[a]Department of Chemical Engineering. Aragon Nanoscience Institute (INA), University of Zaragoza, Spain

[b]CIBER de Bioingeniería, Biomateriales y Nanomedicina, CIBER-BBN, Zaragoza, Spain

[c]Instituto Aragonés de Ciencias de la Salud (IIS Aragon), Centro de Investigación Biomédica de Aragón (CIBA), Zaragoza, Spain

[d]Department of Animal Pathology, Veterinary Faculty, University of Zaragoza, Spain

[e]Instituto de Investigaciones Biomédicas "Alberto Sols", Madrid, Spain

[f]Universidad Francisco de Vitoria, Facultad de Ciencias Biosanitarias, Madrid, Spain

[g]Fundación Araid, 50009 Zaragoza, Spain.

[§]Corresponding author

Email addresses:

P.M.D: p.martin@ufv.es

M.A: arruebom@unizar.es

Abstract

Background

By taking advantage of the preferential engraftment of exogenously administered mesenchymal stem cells (MSCs) in the tumoral stroma, we have demonstrated how those cells can be efficiently used as Trojan horses harbouring plasmonic hollow gold nanoparticles (HGNs) used in photothermal therapy *in vivo*.

Methods

In order to understand the kinetics of the cell internalization process and to calculate the sub-cytotoxic doses of those nanoparticles on MSCs, we have used confocal and scanning-electron microscopy and the Alamar Blue test, respectively. In a first experiment direct intratumoral injections of the nanoparticle-laden cells were used to demonstrate the efficiency of the photothermal therapy. In a second experiment, the therapy efficacy was evaluated either using intravenously administered free plasmonic nanoparticles or the same nanoparticles internalized within MSCs on subcutaneous xenograft tumors.

Results

Under the same irradiation conditions, the ablated surface area after photothermal treatment was ~1.5 times larger when using one single dose of intravenously administered HGN-laden-MSCs compared to the administration of free HGNs.

Conclusions

MSCs are postulated as a better carrier for therapeutical nanoparticles compared to the conventional extravasation into the tumor driven by the enhanced permeability and retention (EPR) effect. Reduced immunogenicity, selective over-accumulation and homogeneous distribution of the nanoparticles around the tumor were observed when using MSCs as “Trojan horses” probably due to the ability of the MSCs to migrate

and integrate homogeneously at sites of inflammation. All these data give enough evidence to consider MSCs as an ideal carrier for nanoparticle-based therapies.

Keywords: Mesenchymal stem cells, cancer, nanoparticles, hyperthermia; photothermal therapy; EPR.

Background

Cancer is the leading cause of death worldwide, with 7.6 million deaths in 2013; data which are projected to continue rising with an estimated 13.1 million deaths in 2030 according to WHO.[1] The increase in the life expectancy, the presence of mutagenic agents in the environment, and the lack of healthy habits could influence this high incidence of the disease.[2]

Preventive medicine, surgery, chemotherapy and radiotherapy are the main approaches to defeat cancer, but they have major side effects because those therapeutical approaches affect both tumoral and healthy tissues. Chemotherapeutic drugs in particular fall short due to not only their unwanted side effects in healthy tissues but also due to the potential development of multidrug resistance and their low permeance towards the interior of the tumor core due to its high interstitial pressure. Therefore, there is a need to develop new, more effective and safer treatments able to reach homogeneously all the tumoral mass, including the central hypoxic regions.

One of the emerging therapies proposed in recent years involves the generation of hyperthermia or tumoral ablation using magnetic or near-infrared (NIR) responsive nanoparticles which generate localized heat by the use of alternating magnetic fields or near infrared (NIR) light, respectively. In this particular application, phototherapy consists on an increase in the local temperature (41-47°C) by using the heat

transmitted by the NIR-absorbing nanoparticles upon laser irradiation, leading to the apoptosis or necrosis of the tumor cells depending on the laser fluence, pulse frequency, wavelength of the irradiating light and irradiation time. Specifically, gold nanoparticles are good candidates to mediate this process because of their high light absorption efficiency, low cytotoxicity, good biocompatibility and their simple and scalable synthesis.[3] Hollow gold nanospheres (HGNs) are able to absorb energy in the NIR region of the electromagnetic spectrum and dissipate it as heat due to electron-electron and electron-phonon relaxations. In addition, between 650 and 1100 nm the absorption and scattering of incident light in biological tissues is reduced. Therefore, in this way, external irradiation of tissues with single wavelength lasers in that region (i.e. 808 nm) produces heat only where the light-absorbing nanoparticles are embedded, reducing the characteristic side effects of other conventional treatments such as chemo- or radiotherapy and to other hyperthermia-based techniques (such as microwave ablation, magnetic fluid ablation, radiofrequency, and focused ultrasound therapy).[4] Compared to other plasmonic nanoparticles such as gold nanorods or core-shell SiO_2-Au nanoparticles, HGNs are more efficient in photothermal therapy for shallow and deep cancers.[4] However, even though there are very efficient nanoparticles as transductors of the NIR light into heat, the use of generalized hyperthermia also produces damage in healthy cells and tissues, and therefore, it is important to obtain local hyperthermia exclusively at the tumor site which it is by no means an easy task.[5] The well known enhanced permeation and retention effect contributes to the passive over-accumulation of nanoparticles at the tumor [6] and selective accumulation can be further increased by the use of suitable antibodies or other recognition biomolecules (carbohydrates, peptides, nucleic acids, etc.) grafted to the external nanoparticle surface.[7] However, a selective

accumulation of nanoparticles requires sufficient circulation time in the bloodstream, but, as it is well known, nanoparticles are rapidly cleared by the macrophages of the reticulo-endothelial system[8] from circulation. To solve this problem, stealthing strategies (e.g. coating with layers of poly-ethylene glycol, biomimetic surface modifications (phosphatidylcholine), etc.) have been developed to increase their circulation life time.[8] In addition, nanoparticles could also be delivered using cells as carriers to evade the immune system recognition ability, in a so-called "Trojan horse" strategy.

This concept of Trojan horse has been postulated in previous works using different nanoparticle-laden cells including dendritic,[9] macrophages[10, 11] and even T lymphocytes.[12] Compared to those previous vectors, bone marrow MSCs have a number of characteristics that make them superior, including their ability for self-renewal, potential to differentiate into different tissues and ability to migrate and integrate at sites of inflammation or into tumors.[13-15] Although the complete mechanism of this phenomenon is still unknown, it is recognized that the release of cytokines in the tumor stroma and their interaction with cytokine and chemokine receptors present in the cell surfaces are involved in the migration of MSCs as well as the adequate hypoxic environment which does not impair their migration.[16] Nanoparticle transport inside MSCs directed against brain tumors was previously demonstrated, although, in that case MSCs were directly injected on site, being the MSCs observed afterwards in the tumor periphery.[17] Dwyer et al.[18] demonstrated a successful engraftment of MSCs at the site of both primary tumors and nodal cancer metastases after systemic administration *in vivo*, although no nanoparticle was carried in that case.

Moreover, MSCs present a great advantage in relation to solve some of the problems found during the nanoparticle-based injection alone such as the previously mentioned rapid immune response and low permeance towards the interior of the tumoral mass due to the high pressure gradient. Regarding to the immune response, the fact that they do not express MHC class II and have a very low expression of MHC class I,[16, 19] may favour the use of these cells in allografts. As it is also known that bone marrow MSCs are able to migrate to hypoxic areas,[16] here we propose the use of these cells as vectors for NIR-responsive nanoparticles to delivery treatment to the central hypoxic areas of tumors by applying optical hyperthermia.

Since sub-cytotoxic doses of cell internalized HGNs are inert in the absence of laser irradiation, this would be a safe protocol that would allow to locally induce hyperthermia at the tumor site. Therefore, here we studied the *in vitro* and *in vivo* behaviour of intravenously injected HGNs and their antitumoral effect in the presence of laser light (808nm) compared to the same nanoparticles internalized within MSCs.

Methods

Synthesis of Hollow Gold Nanospheres.

Nanoparticle synthesis was performed following the protocol described at Preciado-Flores et al. [20] with slight modifications. Briefly, in a two-necked round-bottom flask 400 mL of distilled water, 400 µL of 0.4 M of cobalt chloride hexahydrate ($CoCl_2 \cdot 6H_2O$) and 1.6 mL of 0.1 M sodium citrate trihydrate ($Na_3C_6H_5O_7 \cdot 3H_2O$) were added under an inert Ar atmosphere to avoid a premature Co oxidation. After 40 minutes, 2 mL of a 1 wt. % solution of poly (vinylpyrrolidone) (PVP) with an average Mw of 55000 Da and 400 µL of 1.0 M sodium borohydride ($NaBH_4$) were added. The color change from pale pink to brown was indicative of the cobalt nanoparticle formation. Afterwards, 120 mL of distilled water and 180 µL of 0.1M chloroauric

acid trihydrate ($HAuCl_4 \cdot 3H_2O$) were mixed with 360 mL of the previous cobalt-based dispersion used as a sacrificial template, to promote the formation of $CoCl_2$ and the reduction of Au^{3+} rendering hollow Au-based shells.

The resulting HGNs were coated with poly-ethylene glycol by using an excess of monofunctional poly(ethylene glycol)methyl-ether-thiol (PEG, 1000 Da MW), to take advantage of the strong chemical bond between Au and S[21]. Any excess of unbound PEG was removed by dialysis.

The concentration of the final dispersion was adjusted by centrifugation at 10000 rpm for 10 minutes and both HGNs and PEG-HGNs were thoroughly characterized by transmission electron microscopy, scanning electron microscopy, thermogravimetric analysis (TGA) and UV-visible spectroscopy.

Cell culture conditions

Murine mesenchymal stem cells (MSCs), HeLa cells and human U251MG glioma cells were purchased from Lonza and Cancer Research-UK cell services, respectively. MSCs were cultured in Dulbecco's modified Eagle's F-12 medium (DMEM F-12, GIBCO) with 10% fetal bovine serum (FBS, GIBCO), 1% penicillin/streptomycin and 1% amphotericin and maintained at 37°C in a 5% CO_2-humidified atmosphere under hypoxic conditions (3% O_2). For culturing U251MG and HeLa cells Dulbecco's modified Eagle's medium (DMEM, GIBCO) with 10% fetal bovine serum (FBS, GIBCO), 1% penicillin/streptomycin and 1% amphotericin were used under normoxic conditions.

HGNs cytotoxicity evaluation

The Alamar Blue® is a colorimetric assay to evaluate cell viability and cytotoxicity based on the reduction of resazurin to resorufin by mitochondrial oxidoreductases. During the evaluation, MSCs were seeded into 96-well culture plates at a

concentration of 5 x 10^3 cells per well in 100 µL of the above mentioned medium. After incubation at 37°C in a 5% CO_2-humidified incubator under hypoxic conditions for 24 h, the medium was changed to 100 µL of fresh medium enriched with HGNs (5, 10, 20, 50 and 100 µg mL^{-1}) or with PEG-HGNs (20, 50, 100 and 500 µg mL^{-1}) and cells were cultured for another 24, 48 and 72 h. At these different time points cells were washed with PBS and then treated with 10% (v/v) of resazurin dye reagent prepared in DMEM F-12 medium. Culture plates were then placed in a 37°C/5% CO_2 incubator under hypoxic conditions for 2 h. Afterwards, fluorescence was evaluated at 530/590 nm excitation/emission wavelengths using a Synergy HT (Biotek) plate reader.

Cellular uptake of nanoparticles

Confocal microscopy characterization (Spectral Confocal Microscope Leica TCS SP2) was carried out to evaluate cellular uptake and trafficking on the cells studied. In this case, cells were seed at a density of 3 x 10^4 cells on 20 mm cover slips (in a 24-well plate) and allowed to grow for 2 days. Then HGNs (50 µg mL^{-1}) in DMEM F-12 were added keeping the incubation for 1 day. Finally, cells were fixed with para-formaldehyde 4% and stained with phalloidin to label the cytoplasmic actin. HGN-based agglomerates were directly observed by reflection in the confocal microscope without the need of using fluorophores. For obtaining the SEM Dual-Beam (FEI Nova 200 Dual-Beam SEM/FIB) images cells were dehydrated, dyed and embedded in resin before observation. The electronic observation was combined with a focused ion beam (FIB) to visualize and cut the MSCs. Gallium was used as liquid metal ion source to produce cross-sections of the adherent cells. Both the ion column and the electron column operated at accelerating voltages of 30kV.

Flow cytometry

Nanoparticle internalization was evaluated by using flow cytometry. In this case, 5 mL of HGNs or PEG-HGNs (1mg·mL^{-1}) dispersions were maintained under agitation with Rhodamine 123 (1 mg·mL^{-1}, 25µL) for 1 hour. To remove any potential unbound dye, each dispersion was then dialyzed for two days against distilled water. Afterwards, 1 x 10^6 cells were incubated with the corresponding Rhodamine-labeled nanoparticles and at different time points cells were washed twice with PBS and trypsinized. After centrifugation, cells were then resuspended in PBS (1 x 10^6 cells·mL^{-1}) and analyzed by flow cytometry with an ImageStreamX (Seattle, WA, USA).

Cell irradiation

To study the laser effect in the cells containing sub-cytotoxic doses of internalized HGNs, MSCs (50000-100000 cells/well) were incubated with the HGNs (0,02 or 0,05 mg·mL^{-1}) during one day. After that, those adherent cells were washed twice with PBS, to ensure that any possible heating would not be produced by free, non-internalized nanoparticles present in the medium. MSCs were then irradiated in DMEM F-12 during 30 minutes with a NIR laser (808 nm) at 1W·cm^{-2} of irradiance. Then, irradiated cells were incubated in a 37°C/5% CO_2 incubator under hypoxic conditions for 48 h. After that time cells were incubated with the LIVE/DEAD® fluorescent reagent (Life Technologies) following the manufacturer's protocol and visualized under an inverted fluorescence microscope (Olympus IX81). The Alamar Blue® assay was also used in order to compare the viability of the irradiated cells with and without internalized nanoparticles.

In vivo experiments

All procedures were carried out under Project License PI 14/11 approved by the in-house Ethic Committee for Animal Experiments from the University of Zaragoza. The care and use of animals were performed accordingly with the Spanish Policy for Animal Protection RD53/2013, which meets the European Union Directive 2010/63 on the protection of animals used for experimental and other scientific purposes.

For these experiments six- to eight-week-old female BALB/c nu/nu mice (Harlan Iberica) were used. All the animals received subcutaneous injections of 5 x 10^6 U251MG cells or HeLa cells suspended in 200 µl of PBS for the generation of subcutaneous xenograft tumors. When the tumor size was >0.5cm^2, the animals were divided into groups of four mice per group.

In the first experiment direct intratumoral injections of the nanoparticle-laden cells (HGNs and PEG-HGNs) were used to demonstrate the efficiency of the photothermal therapy, with five experimental groups. In this case, all groups were injected with 5 x 10^6 HeLa cells in one flank of the mouse for tumor induction. Group 1 included control animals which did not receive any treatment; Group 2 received laser irradiation but not HGNs injection; Group 3 received HGNs injection (50µg) but not laser irradiation; Group 4 received HGNs (50µg) carried by 10^6 MSCs and laser irradiation and Group 5 received both HGNs (50 µg) and laser. After one day of nanoparticle or MSC administration these two last groups and the control were irradiated with a NIR-laser (808nm) at an irradiance of 1$W \cdot cm^{-2}$ during 5 min. Tumor size was periodically evaluated by using a caliper up to 15 days after irradiation.

The second experiment was aimed to assess the efficiency of MSCs as carriers of HGNs compared to conventional intravenous administration of plasmonic nanoparticles. To this end, we divided the animals into four groups. The first group served as control. The second group received an intravenous injection of 100 µg PEG-

HGNs in 100 µl of PBS through the tail vein. The third and fourth groups were injected with a suspension of 1 x 10^6 MSCs separately loaded with 100 µg PEG-HGNs in 100 µL of PBS. Previously, cells were incubated with the PEG-HGNs for 24 hours, and afterwards cells were washed, trypsinized and one million of MSCs containing nanoparticles were injected in the tail vein.

One day after intravenous injection, the second and third groups were irradiated during 5 min with a NIR laser (808 nm) at $1W \cdot cm^{-2}$ irradiance around all the tumoral area using a spot size larger than the tumor projected surface. The fourth group did not receive any laser irradiation. One week after intravenous injection the same dose of irradiation was used again following the same protocol. Tumor size evolution was evaluated over two weeks, until the tumor size was as big as the maximum size permitted by the University ethics committee. At this time point, animals were euthanized by CO_2 inhalation. Tumor, brain, heart, kidney, liver, lung, spleen and gastrointestinal organs were collected from each animal for histopathological analysis and to evaluate gold bioaccumulation by ICP-MP-AES (4100, Agilent).

Statistical analysis

All experiments were repeated in triplicate unless otherwise stated. Statistical evaluation of data was carried out using the SPSS Statistics software package (version 17.0; IBM SPSS, Chicago, IL, USA). For the non-normal distributions the Mann-Whitney U test was carried out. In all tests, $P<0.05$ was regarded as statistically significant.

Tissue analysis

Tissues were formalin-fixed and processed using routine histological methods. Sections of 3 µm were prepared after paraffin embedding and the slides were stained with hematoxylin and eosin. Microscopic lesions were described and a mitotic activity

index was calculated by counting mitotic figures in ten consecutive high-power fields (HPF, 40x) from the most densely packed cellular area of the corresponding sample. To evaluate the proliferation index, an immunohistochemical analysis with Ki-67 (FLEX monoclonal mouse anti-human Ki67 clone MIB-1 from DAKO, Denmark) was performed. Sections were incubated at room temperature with primary antibodies for 20 min at pH 6. The Envision Flex/Hrp Dako™ visualization system was used followed by a counterstaining with hematoxylin. Negative control sections received only antibody diluent instead of the primary antibody. Ki-67 expression was evaluated in all groups by counting positive and negative cells in ten consecutive HPF using the ImageJ software. On those images, the percentage of positive cells and their confidence interval (95%) were calculated.

Organs and tumors were digested by dissolving them in hydrochloric:nitric acid (3:1) in a Teflon-lined digester using a Milestone ETHOS Plus Srl (Sorisole, Bergamo, Italy) microwave at 195 ºC. Digested samples were diluted and gold content analyzed by ICP-MP-AES (4100, Agilent). Elemental gold standard (TraceCERT®, 1000 mg/L Au in hydrochloric acid, Fluka) was used for calibration.

Results and Discussion

Spherical hollow gold nanoparticles with 40,5 ± 7 nm in diameter (Figure 1A-C), were obtained after galvanic replacement using cobalt oxide nanoparticles as templates. Both HGNs and PEG-HGNs showed a characteristic localized surface plasmon resonance peak in the NIR region (Figure 1D). A slight blue shift was observed for the pegylated nanoparticles, possibly attributed to a different dielectric value in the interfacial double layer coating the nanoparticles in agreement with the previous literature.[22] The amount of PEG on the surface of the HGNs was 12 $\mu g \cdot g^{-1}$, evaluated by TGA.

Compared to the control, PEG-HGNs did not decrease the cell viability at the doses tested (20, 50, 100 and 500 $\mu g \cdot mL^{-1}$) (Figure 2A). Our results are in agreement with previous studies which demonstrate that nanoparticle cytotoxicity is reduced after pegylation.[23] Also, this reduced cytotoxicity is in agreement with previous reports for MSCs harboring HGNs which also indicate that those nanoparticles did not affect MSCs differentiation.[24] A dose-dependent cytotoxicity was observed for the bare HGNs with a marked decrease in the cell viability at doses above 50 $\mu g\ mL^{-1}$ after 24h of incubation. It is important to point out that the apparent increase in cell viability observed after 72h of incubation is caused by the normalization selected for the control because we used the total number of viable cells remaining after 72 h as control. Obviously the total number of cells after 72 h was lower than the numbers obtained for the other times studied (0, 24 and 48h).

Nanoparticle cell trafficking was evaluated by using confocal microscopy, scanning electron microscopy, flow cytometry and ICP. For the confocal studies, cells were permeabilized and stained with Draq5 to label the nuclei and with phalloidin-Alexa488 to stain the cytoskeletal actin fibers. Due to their agglomeration in endocytic vesicles, HGNs were observed by using the reflection mode of the mciroscope exciting at 488 nm and collecting the emission between 479 and 498 nm. Z-stack orthogonal projections were carried out in order to demonstrate the presence of the nanoparticles inside the cytosol (Figure 3). HGNs internalization was also demonstrated by using SEM Dual-Beam (Figure 2B). Nanoparticles were clearly internalized forming aggregates inside vesicles, probably following the endosomal route, and the phenomenon was observed even after 7 days of co-incubation (Figure 4). Differences in the internalization dynamics were found using flow cytometry by labelling the bare and PEGylate nanoparticles with rhodamine123. A maximum

nanoparticle internalization was reached at 24 and at 72 hours for the PEG-HGNs and the HGNs, respectively. It is important to point out that the chemical bond (Au-N) between rhodamine123 and gold through the lone pair electrons at the amino groups discards the potential detachment of the dye from the nanoparticles [25].

In the intratumoral (first) experiment, the treated groups were injected either with 50μg of HGNs or with one million of MSCs co-incubated with 50μg of HGNs during 72h. At this time point the amount of nanoparticles detected in the digested cells was 33 μg (evaluated by ICP). Tumors in Group 5 (HGNs+laser) reduced completely their size one week after irradiation (Figure 5). This result reflects the efficiency of the plasmonic HGNs in releasing heat locally after NIR irradiation. Since in this experiment, the HGNs were injected stereotactically, most of the HGN-based dose will be located and accumulated in the proximity of the tumor. Tumor sizes in Group 4 (MSCs + HGNs +laser) strongly decreased (~ 80% reduction in the projected area by day 12), but the tumor reduction was not as high as the one observed for Group 5 due to the lower dose of plasmonic nanoparticles transported by the MSCs. In all other control groups tumor sizes increased. Figure 5a shows the evolution of the projected area of the tumor over time. Our results show that optical hyperthermia reduces the size of the tumor in only one week after treatment when a direct intra-tumoral injection is used whereas, in other works, the combined use of intravenously administered NIR-responsive nanoparticles and chemotherapy produces also a complete tumor remission 20 days after irradiation.[26]. Therefore, the route of administration plays a key role in the dynamic process of over-accumulating a therapeutic dose of plasmonic nanoparticles in the tumoral area.

On a second experiment (Figure 6) and after the demonstration that HGNs were able to mediate tumor regression, we administered the nanoparticles via intravenous

injection in the tail of the corresponding mouse. In this case, in order to reduce the number of animals we divided the animals into four groups. The control groups were the use of MSCs with PEG-HGNs but without any laser application and one additional control without any treatment. We used either PEG-HGNs or MSCs harboring PEG-HGNs in the other groups. As we mentioned before, MSCs can migrate to sites of injury and inflammation,[13] so we used these cells intravenously to analyze their capability in over-accumulating sub-cytotoxic doses in hypoxic and inflamed diseased tissues. Instead of bare HGNs, PEG-HGNs were used and delivered to tumors in order to reduce the recognition and fast clearance of the bare nanoparticles by the immune system. In this experiment we used U251MG glioma cells as a model tumor, because of the aggressiveness of this cell line, as we thought that the treatment on those tumors would be a major challenge than the previous HeLa-based model used in the first experiment.

All groups were injected with 5 x 10^6 U251MG cells in one flank of the mouse for tumor induction. In this case, and compared to the previous experiment, we injected in the tail of the mouse a higher dose of PEG-HGNs (100 µg/per animal) or one million MSCs/animal loaded with 100 µg (evaluated by ICP) of PEG-HGNs, because the amount of gold per unit mass of nanoparticles coated with PEG was lower than that for the nanoparticles without coating due to the PEG corona. In this case, one day after the injection, tumors were irradiated. At this time point we could see a dark staining at the tumor site on mice where PEG-HGNs (either alone or vehiculizated) were used. Those observations did not take place for the control groups, indicating that part of the PEG-HGNs had already reached the tumor probably due to the EPR effect. These results are in agreement with previous works in which it was demonstrated that metal nanoparticles accumulate immediately in the tumor *in vivo*

using dynamic imaging studies.[27, 28] One week after the intravenous injection we irradiated the tumors again, because, as it was previously reported, it takes approximately one week for bone marrow MSCs to accumulate in the tumoral area.[29]

Tumor development was followed until mice carried tumors at the ethically allowed size. At the end of the experiment the size of the tumor in the group with MSCs + PEG-HGNs and laser irradiation showed a higher decrease in the projected area compared to the group treated with PEG-HGNs and laser only without cells. This suggests that MSCs have been able to carry the nanoparticles to the tumors more efficiently than the well known extravasation achieved thanks to the EPR effect when using non-shuttled nanoparticles. The heterogeneity of the EPR effect in human cancers, including uncertainty in the degree of its effect in clinical cases has been widely reported in the literature.[30] Our results are in agreement with the work of Zhang et al.[24] who demonstrated a co-localization of human MSCs loaded with HGNs around tumoral blood vessels. In the group with PEG-HGNs and laser only the final tumor projected area was smaller than in the control corroborating the efficiency of the photothermal therapy. But, as we demonstrated, this efficiency can be boosted when using MSCs as carriers of the plasmonic gold nanoparticles. In the group with MSCs + PEG-HGNs without laser no significant differences were observed in the total tumor projected area compared to the one measured for the control. Smith et al.[30] have recently reported how intravenous administered carbon nanotubes might be uptaken by a specific subset of circulating inflammatory monocytes which carry them into the tumor. Therefore, not only the extravasation and over-accumulation due to the EPR effect are necessary to consider when taking about direct intravenous injection of nanomaterials but also a monocyte-based transport. However the ability

of MSCs to engraft in the tumoral stroma can be used to achieve higher doses of therapeutic nanoparticles in the target.

The histological studies demonstrated that all the tumors showed an expansive, non-encapsulated, highly cellular neoplastic proliferation composed of extensive sheets of polyhedral, highly pleomorphic cells with atypical mitosis. Tumor cells showed round to ovoid nuclei, prominent nucleoli and a moderated, ill-defined eosinophylic cytoplasm. In those cells the stroma was formed by a scant connective tissue.

As shown in Figure 7, all groups (G1-G4) showed tumor masses with a central necrotic area. Interestingly, whereas G1 (control) and G4 (MSCs + PEG-HNPs without laser) tumors presented a single central area of necrosis, G2 (PEG-HNPs + laser) and G3 (MSCs + PEG-HNPs with laser) tumors showed additionally extensive multifocal necrotic areas within peripheral, viable tumor parenchyma. Regarding the mitotic activity index, G1 and G4 tumors showed a mean of 15 mitotic figures/10 HPF whereas the mean for G2 and G3 tumors was 9 mitotic figures/10 HPF. Globally, these results might indicate increased treatment efficiency in those tumors containing nanoparticles and receiving laser irradiation.

The immunohistochemical analysis on the central area of the tumors recovered at the end of the experiment for Ki-67 expression indicated that G2 and G3 tumors exhibited lower expression of the protein when compared to G1 and G4 tumors (Table 1), being the difference on the protein expression between G2 and G3, G3 and G1, and G2 and G1, statistically significant ($p<0.05$). Ki-67 is a nuclear antigen expressed only in the different phases of cellular division, and therefore, it is widely used proliferation biomarker to estimate growth rates. In this regard, Ki-67 expression can also be used as a prognostic indicator of cerebral high-grade glioblastomas.[31] These histological

results support the possibility of a better prognosis for tumors subjected to this therapy, especially on the group treated with MSCs+ PEG-HGNs+ laser.

No lesions were found in all remaining organs studied (brain, heart, kidney, liver, lung, spleen and gastrointestinal organs), denoting the lack of systemic injuries by the proposed localized treatment. ICP-OES analysis did not detect gold at any dose above the detection limit of the system ($50 \mu g \cdot L^{-1}$) in any of the groups probably because after 27 days (the total number of days from the injection) the nanoparticles were mostly cleared from the tumor site which represents a very positive result considering that nanoparticles with optimal clearance characteristics will minimize toxicity risks. This result was also not surprising considering that it has been reported that the gold content in the tumor tissue amounts to ~1 % of its concentration in the injected suspensions.[32]

Conclusions

Hollow gold nanoparticles are efficient transducers *in vivo* of near infrared light into heat when stereotactically injected into subcutaneous HeLa cell-line xenograft tumors of when intravenously administered in the treatment of subcutaneous U251MG cell-line xenograft tumors. The heterogeneity of the EPR effect in human cancers leads to a variable distribution of plasmonic nanoparticles within the tumor, probably due to the degree of necrosis in solid tumors and a reduced lymphatic drainage. Also, it seems likely that in spite of the PEG coating, a fraction of the free HGNs injected intravenously will be detected and cleared by RES macrophages providing a relatively modest specificity towards the tumoral mass. Both problems were alleviated by using MSCs as carriers of those nanomaterials.

A successful subcytotoxic internalization of both bare and PEGylated hollow gold nanoparticles was demonstrated in murine MSCs using confocal and scanning

electron microscopy and also ICP analysis. Taking advantage of the tumor-homing ability of nanoparticle-loaded MSCs, a homogeneous nanoparticle distribution across the tumoral tissue was obtained and this phenomenon led to tumor eradication when applying photothermal therapy. Therefore, PEGylated hollow gold nanoparticles internalized within MSCs are efficient photothermal therapeutic agents on subcutaneous xenograft glioma. The immunohistochemical analysis revealed increased treatment efficiency in those tumors containing nanoparticles and receiving laser irradiation, especially on the group treated with nanoparticle-laden MSCs. The preferential accumulation of those carriers in the tumor blood vessels might be responsible for a homogeneous distribution along all the tumoral mass and a consequent efficient photothermal outcome.

Authors' contributions

MME performed most of the experimental procedures, collected the data, made the calculations and participated in the manuscript writing. MME, LG, and VS participated in the experimental procedures, calculations and analysis. LL and MG performed the pathological studies. PMD and MQ participated in the *in vivo* studies. MME, PMD, MA and JSM were responsible of the conception and design of the study and wrote the manuscript.

Acknowledgements

Financial support from the EU thanks to the ERC Consolidator Grant program (ERC-2013-CoG-614715, NANOHEDONISM) and the EU CIG–Marie Curie under the REA grant agreement no. 321642 are gratefully acknowledged.

We are grateful to the Scientific Services of the Aragon Institute of Health Sciences, specifically to the Cytometry and Cell Sorting Services and to the Microscopy and

Pathology Services and their specialists: César Vallejo, Javier Godino, María Royo, Amparo Gallur, María Luisa Bernad and Cyndi Giraldo.

References

1. Jemal A, Bray F, Center MM, Ferlay J, Ward E, Forman D: **Global Cancer Statistics**. *Ca-Cancer J Clin* 2011, **61**(2):69-90.
2. **World Health Organization. Cancer. Fact sheet N°297** [http://www.who.int/mediacentre/factsheets/fs297/en/).]
3. Li J, Gupta S, Li C: **Research perspectives: gold nanoparticles in cancer theranostics**. *Quant Imaging Med Surg* 2013, **3**(6):284-291.
4. Kessentini S, Barchiesi D: **Quantitative comparison of optimized nanorods, nanoshells and hollow nanospheres for photothermal therapy**. *Biomed Opt Express* 2012, **3**(3):590-604.
5. Takagi H, Azuma K, Tsuka T, Imagawa T, Osaki T, Okamoto Y: **Antitumor effects of high-temperature hyperthermia on a glioma rat model**. *Oncol Lett* 2014, **7**(4):1007-1010.
6. Chisholm EJ, Vassaux G, Martin-Duque P, Chevre R, Lambert O, Pitard B, Merron A, Weeks M, Burnet J, Peerlinck I *et al*: **Cancer-Specific Transgene Expression Mediated by Systemic Injection of Nanoparticles**. *Cancer Res* 2009, **69**(6):2655-2662.
7. Dawidczyk CM, Kim C, Park JH, Russell LM, Lee KH, Pomper MG, Searson PC: **State-of-the-art in design rules for drug delivery platforms: Lessons learned from FDA-approved nanomedicines**. *J Control Release* 2014, **187**:133-144.
8. Chithrani DB: **Intracellular uptake, transport, and processing of gold nanostructures**. *Mol Membr Biol* 2010, **27**(7):299-311.
9. Matsuo K, Ishii Y, Matsuo K, Yoshinaga T, Akashi M, Mukai Y, Yoshioka Y, Okada N, Nakagawa S: **The Utility of Poly(gamma-glutamic acid) Nanoparticles as Antigen Delivery Carriers in Dendritic Cell-Based Cancer Immunotherapy**. *Biol Pharm Bull* 2010, **33**(12):2003-2007.
10. Choi J, Kim HY, Ju EJ, Jung J, Park J, Chung HK, Lee JS, Lee JS, Park HJ, Song SY *et al*: **Use of macrophages to deliver therapeutic and imaging contrast agents to tumors**. *Biomaterials* 2012, **33**(16):4195-4203.
11. Baek SK, Makkouk AR, Krasieva T, Sun CH, Madsen SJ, Hirschberg H: **Photothermal treatment of glioma; an in vitro study of macrophage-mediated delivery of gold nanoshells**. *J Neuro-Oncol* 2011, **104**(2):439-448.
12. Steinfeld U, Pauli C, Kaltz N, Bergemann C, Lee HH: **T lymphocytes as potential therapeutic drug carrier for cancer treatment**. *Int J Pharm* 2006, **311**(1-2):229-236.
13. Belmar-Lopez C, Mendoza G, Oberg D, Burnet J, Simon C, Cervello I, Iglesias M, Ramirez JC, Lopez-Larrubia P, Quintanilla M *et al*: **Tissue-derived mesenchymal stromal cells used as vehicles for anti-tumor therapy exert different in vivo effects on migration capacity and tumor growth**. *Bmc Med* 2013, **11**.
14. Uchibori R, Tsukahara T, Ohmine K, Ozawa K: **Cancer gene therapy using mesenchymal stem cells**. *Int J Hematol* 2014, **99**(4):377-382.

15. Sadhukha T, O'Brien TD, Prabha S: **Nano-engineered mesenchymal stem cells as targeted therapeutic carriers**. *J Control Release* 2014, **196**:243-251.
16. Annabi B, Lee YT, Turcotte S, Naud E, Desrosiers RR, Champagne M, Eliopoulos N, Galipeau J, Beliveau R: **Hypoxia promotes murine bone-marrow-derived stromal cell migration and tube formation**. *Stem Cells* 2003, **21**(3):337-347.
17. Roger M, Clavreul A, Venier-Julienne MC, Passirani C, Sindji L, Schiller P, Montero-Menei C, Menei P: **Mesenchymal stem cells as cellular vehicles for delivery of nanoparticles to brain tumors**. *Biomaterials* 2010, **31**(32):8393-8401.
18. Dwyer RM, Potter-Beirne SM, Harrington KA, Lowery AJ, Hennessy E, Murphy JM, Barry FP, O'Brien T, Kerin MJ: **Monocyte chemotactic protein-1 secreted by primary breast tumors stimulates migration of mesenchymal stem cells**. *Clin Cancer Res* 2007, **13**(17):5020-5027.
19. Loebinger MR, Janes SM: **Stem cells as vectors for antitumour therapy**. *Thorax* 2010, **65**(4):362-369.
20. Preciado-Flores S, Wang DC, Wheeler DA, Newhouse R, Hensel JK, Schwartzberg A, Wang LH, Zhu JJ, Barboza-Flores M, Zhang JZ: **Highly reproducible synthesis of hollow gold nanospheres with near infrared surface plasmon absorption using PVP as stabilizing agent**. *J Mater Chem* 2011, **21**(7):2344-2350.
21. Brust M, Walker M, Bethell D, Schiffrin DJ, Whyman R: **Synthesis of Thiol-Derivatized Gold Nanoparticles in a 2-Phase Liquid-Liquid System**. *J Chem Soc Chem Comm* 1994(7):801-802.
22. Goodman AM, Cao Y, Urban C, Neumann O, Ayala-Orozco C, Knight MW, Joshi A, Nordlander P, Halas NJ: **The surprising in vivo instability of near-IR-absorbing hollow Au-Ag nanoshells**. *ACS Nano* 2014, **8**(4):3222-3231.
23. Diaz B, Sanchez-Espinel C, Arruebo M, Faro J, de Miguel E, Magadan S, Yague C, Fernandez-Pacheco R, Ibarra MR, Santamaria J *et al*: **Assessing Methods for Blood Cell Cytotoxic Responses to Inorganic Nanoparticles and Nanoparticle Aggregates**. *Small* 2008, **4**(11):2025-2034.
24. Zhang YS, Wang Y, Wang LD, Wang YC, Cai X, Zhang C, Wang LHV, Xia YN: **Labeling Human Mesenchymal Stem Cells with Gold Nanocages for in vitro and in vivo Tracking by Two-Photon Microscopy and Photoacoustic Microscopy**. *Theranostics* 2013, **3**(8):532-543.
25. Yajima T, Yu YY, Futamata M: **Closely adjacent gold nanoparticles linked by chemisorption of neutral rhodamine 123 molecules providing enormous SERS intensity**. *Phys Chem Chem Phys* 2011, **13**(27):12454-12462.
26. You J, Zhang R, Zhang GD, Zhong M, Liu Y, Van Pelt CS, Liang D, Wei W, Sood AK, Li C: **Photothermal-chemotherapy with doxorubicin-loaded hollow gold nanospheres: A platform for near-infrared light-trigged drug release**. *J Control Release* 2012, **158**(2):319-328.
27. Tucker-Schwartz JM, Beavers KR, Sit WW, Shah AT, Duvall CL, Skala MC: **In vivo imaging of nanoparticle delivery and tumor microvasculature with multimodal optical coherence tomography**. *Biomed Opt Express* 2014, **5**(6):1731-1743.
28. Laurent S, Dutz S, Hafeli UO, Mahmoudi M: **Magnetic fluid hyperthermia: Focus on superparamagnetic iron oxide nanoparticles**. *Adv Colloid Interfac* 2011, **166**(1-2):8-23.

29. Latorre-Romero C, Marin-Yaseli MR, Belmar-Lopez C, del Moral R, Marijuan PC, Quintanilla M, Martin-Duque P: **Using living cells to transport therapeutic genes for cancer treatment**. *Clin Transl Oncol* 2011, **13**(1):10-17.
30. Smith BR, Ghosn EEB, Rallapalli H, Prescher JA, Larson T, Herzenberg LA, Gambhir SS: **Selective uptake of single-walled carbon nanotubes by circulating monocytes for enhanced tumour delivery**. *Nat Nanotechnol* 2014, **9**(6):481-487.
31. Mastronardi L, Guiducci A, Puzzilli F, Ruggeri A: **Relationship between Ki-67 labeling index and survival in high-grade glioma patients treated after surgery with tamoxifen**. *Journal of neurosurgical sciences* 1999, **43**(4):263-270.
32. Terentyuk GS, Ivanov AV, Polyanskaya NI, Maksimova IL, Skaptsov AA, Chumakov DS, Khlebtsov BN, Khlebtsov NG: **Photothermal effects induced by laser heating of gold nanorods in suspensions and inoculated tumours during in vivo experiments**. *Quantum Electron*+ 2012, **42**(5):380-389.

Figures

Figure 1 - Characterization of the photothermal nanoparticles

(A) TEM images for Hollow Gold Nanospheres. Scale bars, 50 nm (top) and 20 nm (bottom). (B) STEM-HAADF images of Hollow Nanospheres. Scale bars, 20 nm (top) and 5 nm (bottom). (C) TEM images of PEG-Hollow Gold Nanospheres. The halo around the nanoparticles demonstrates the PEG coating. In this case, phosphotungstic acid was used to dye the polymer and allow TEM observation. Scale bars, 50 nm (left) and 20 nm (right). (D) UV-Vis extinction spectra of HGNs and PEG-HGNs.

Figure 2 - Cytotoxicity and cell trafficking studies

A) Graphs showed AlamarBlue assays results for HGNs and PEG-HGNs, respectively. For the experiments with HGNs, 20 $\mu g \cdot mL^{-1}$ was chosen as the highest dose which did not induce cytotoxicity. For the PEG-HGNs case we used 50 $\mu g \cdot mL^{-1}$ as limit of the sub-cytotoxic dose. (B) Dual Beam images demonstrate that the nanoparticles locate inside the cells. The two images above correspond to a MSC

photographs at different magnifications. In the bottom left image a cross section of a cell shows the presence of HGNs, the zoom showed in the right panel shows the morphology of those aggregates. EDX analysis on those aggregates corroborates the presence of Au inside the cell. Scale bars, 20 µm (top left), 10 µm (top right), 5 µm (bottom) and 300 nm (bottom).

Figure 3 - Nanoparticle internalization within MSCs

(A) Confocal Z-Stack. Scale bar: 75 µm. Red dots correspond to the HGNs in the cell after 24 h of incubation with PEG-HGNs. (B) SEM backscattered image. Scale bar: 10 µm (left) and 5 µm (right). EDX revealed that the atomic composition of those aggregates corresponds to gold (results not shown).

Figure 4 - Flow cytometry based kinetics of the internalization process

(A) Nanoparticle internalization kinetics of HGNs (top) and PEG-HGNs (bottom). (B) Image of the flow cytometer showing control cells (top) and rhodamine labelled gold nanoparticles loaded within MSCs MSCs (bottom).

Figure 5 - Photothermal therapy on HeLa cell-line xenograft tumors after intratumoral administration

In vivo antitumoral activity on HeLa tumors. (A) Tumor size evolution over time for both treated and control groups. (B) Photographs of HeLa xenografts at day 12 after laser irradiation. It is important to point out that the projected laser-spot size was larger than the size of the projected area of the tumors.

Figure 6 - Photothermal therapy on U251MG cell-line xenograft tumors after intravenous administration

(A) Tumor size evolution over time for both treated and control groups. The first arrow indicates the time in which HGNs or HGNs-loaded in MSCs were administered, the second and the third arrows show the time span in which the laser

irradiation took place. (B) Tumor area of the different groups at day 20 after the injection. The differences between control and the groups marked with * were statistically significant ($P<0.05$). (C) Photographs of U251MG xenografts at day 12 after the first laser irradiation. It is important to point out that the projected laser-spot size used was larger than the size of the projected area of the tumors.

Figure 7 - Hematoxilin-eosin staining results for histological sections recovered at the end of the experiment

(A-D). Ki-67 staining (E-F). (A) Control tumor (G1 group). Highly cellular pleomorphic neoplastic proliferation. H&E 10x. (B) PEG-HGNs+ laser treated tumor (G2 group). Multifocal necrotic areas on the tumor parenchyma. H&E 4x. (C) MSCs+ PEG-HGNs+ laser treated tumor (G3 group). Focally extensive necrotic area affecting most of the tumor parenchyma. H&E 4x. (D) MSCs+ PEG-HGNs (G4 group). Highly cellular, expansive neoplastic proliferation. H&E 4x. (E) Control tumor (G1 group). Positive staining for Ki-67 on 78% of neoplastic cells. IHQ 10x. (F) MSCs+ PEG-HGNs+ laser treated (G3 group). Positive staining for Ki-67 on 59% of neoplastic cells. IHQ 10x.

Tables

Table 1 - Immunohistochemical staining for Ki-67 expression on tumor cells

Groups	% Ki67 positive cells	% Ki67 negative cells
Control (G1)	**78%**	**22%**
PEG-HGNs + laser (G2)	**66%**	**34%**
MSCs + PEG-HGNs + laser (G3)	**59%**	**41%**
MSCs + PEG-HGNs (G4)	**76%**	**24%**

Additional files

Additional file 1 – Supplementary results

Additional information is available in the Supplementary results section.

SYNOPSIS TOC

Use Of Gold Nanoparticles In Tumor Phototherapy By Employing Mesenchymal Stem Cells As Selective Trojan-Horses.

M. Mar Encabo-Berzosa, Marina Gimeno, Lluís Luján, Leyre Gómez , Victor Sebastian, Miguel Quintanilla, Manuel Arruebo, Jesús Santamaría, Pilar Martín-Duque.

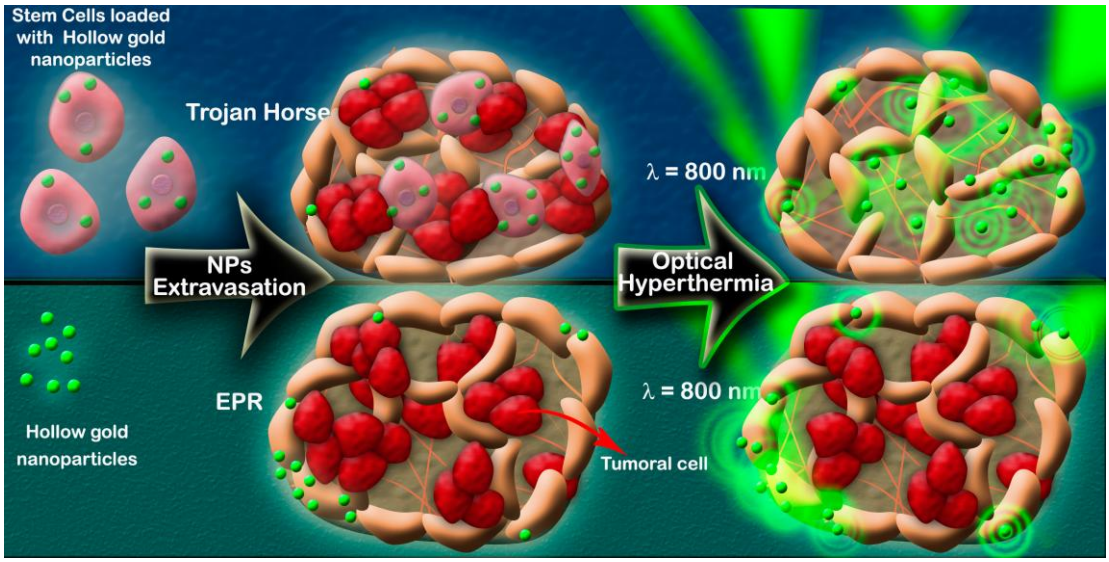

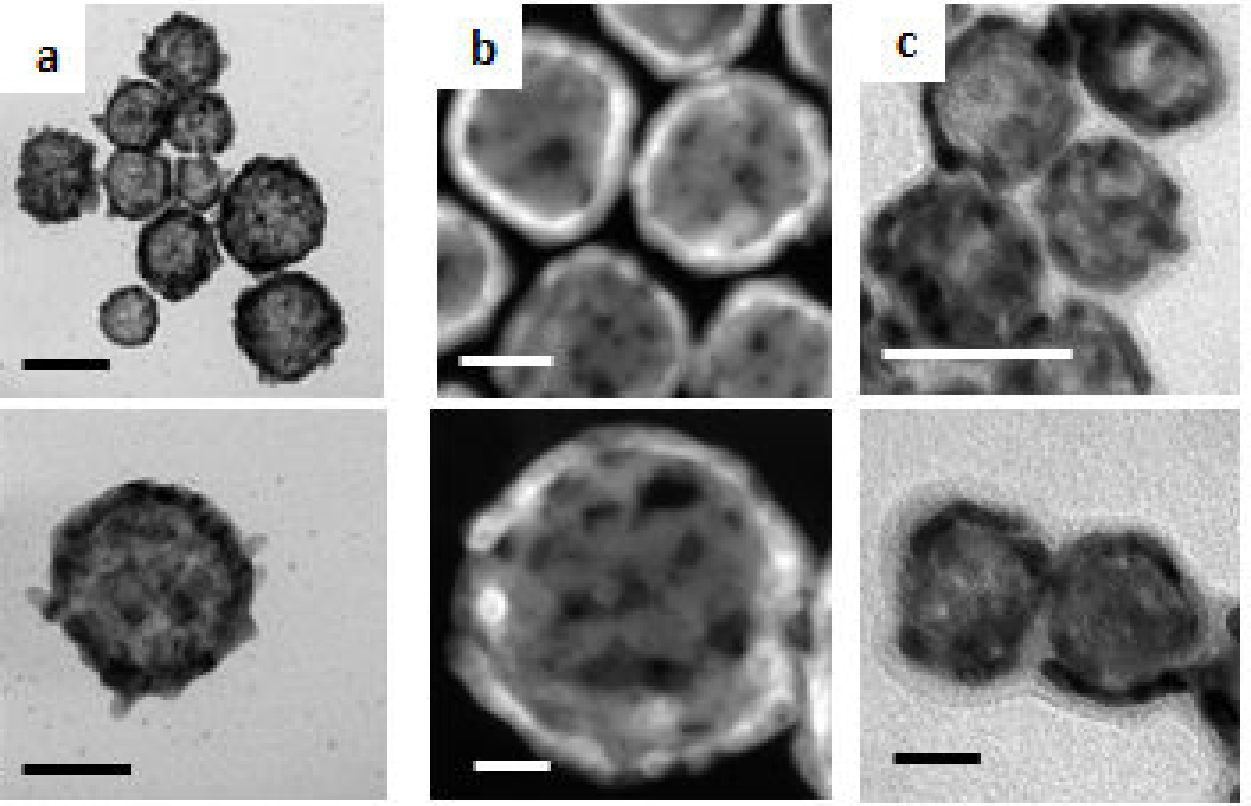
a
b
c

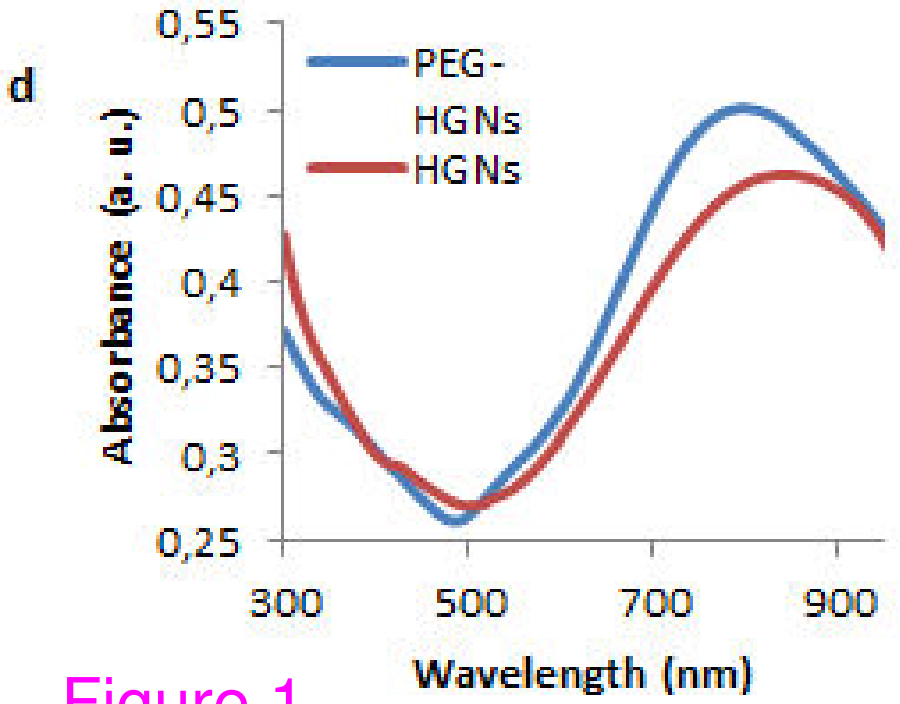
d
0,55
0,5
0,45
0,4
0,35
0,3
0,25
Absorbance (a. u.)
PEG-HGNs
HGNs
300
500
700
900
Wavelength (nm)

Figure 1

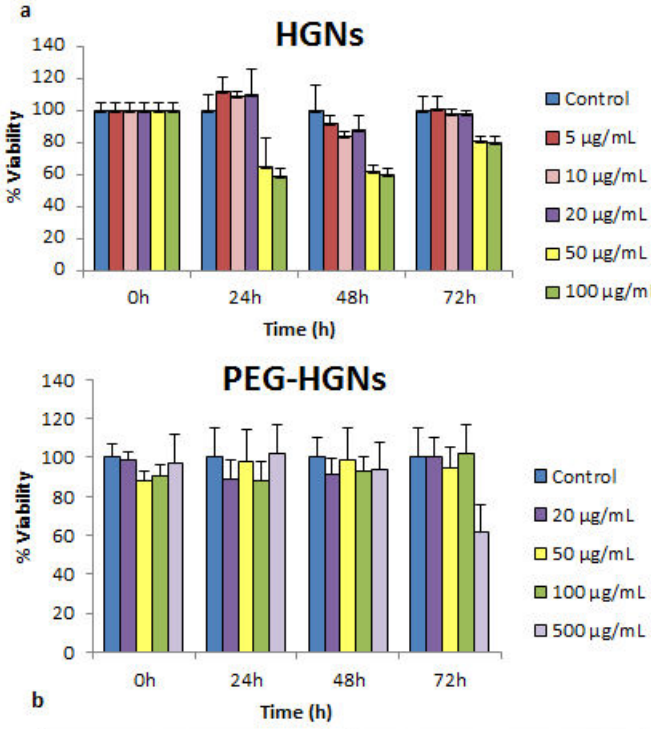
a
HGNs
% Viability
140
120
100
80
60
40
20
0
0h
24h
48h
72h
Time (h)
Control
5 µg/mL
10 µg/mL
20 µg/mL
50 µg/mL
100 µg/mL
PEG-HGNs
% Viability
140
120
100
80
60
40
20
0
0h
24h
48h
72h
Time (h)
Control
20 µg/mL
50 µg/mL
100 µg/mL
500 µg/mL

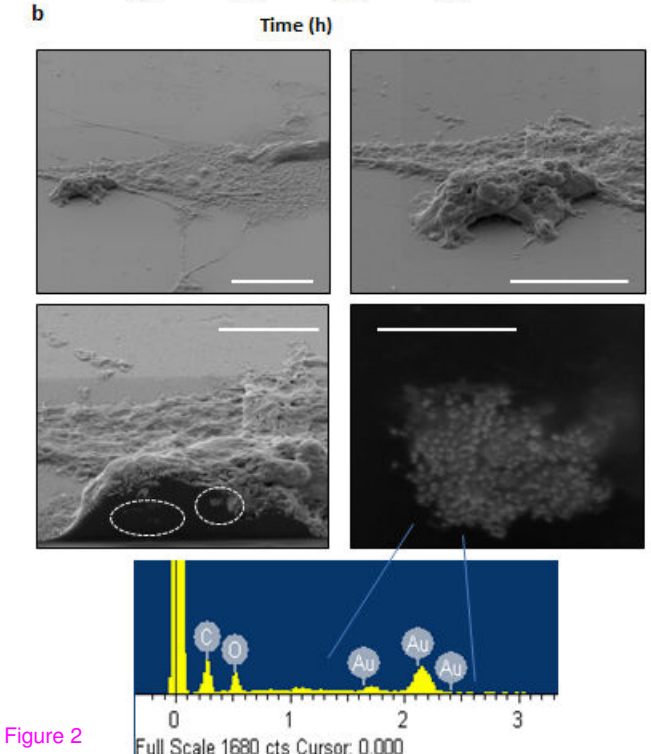
b
C
O
Au
Au
Au
0
1
2
3
Full Scale 1680 cts Cursor: 0.000

Figure 2

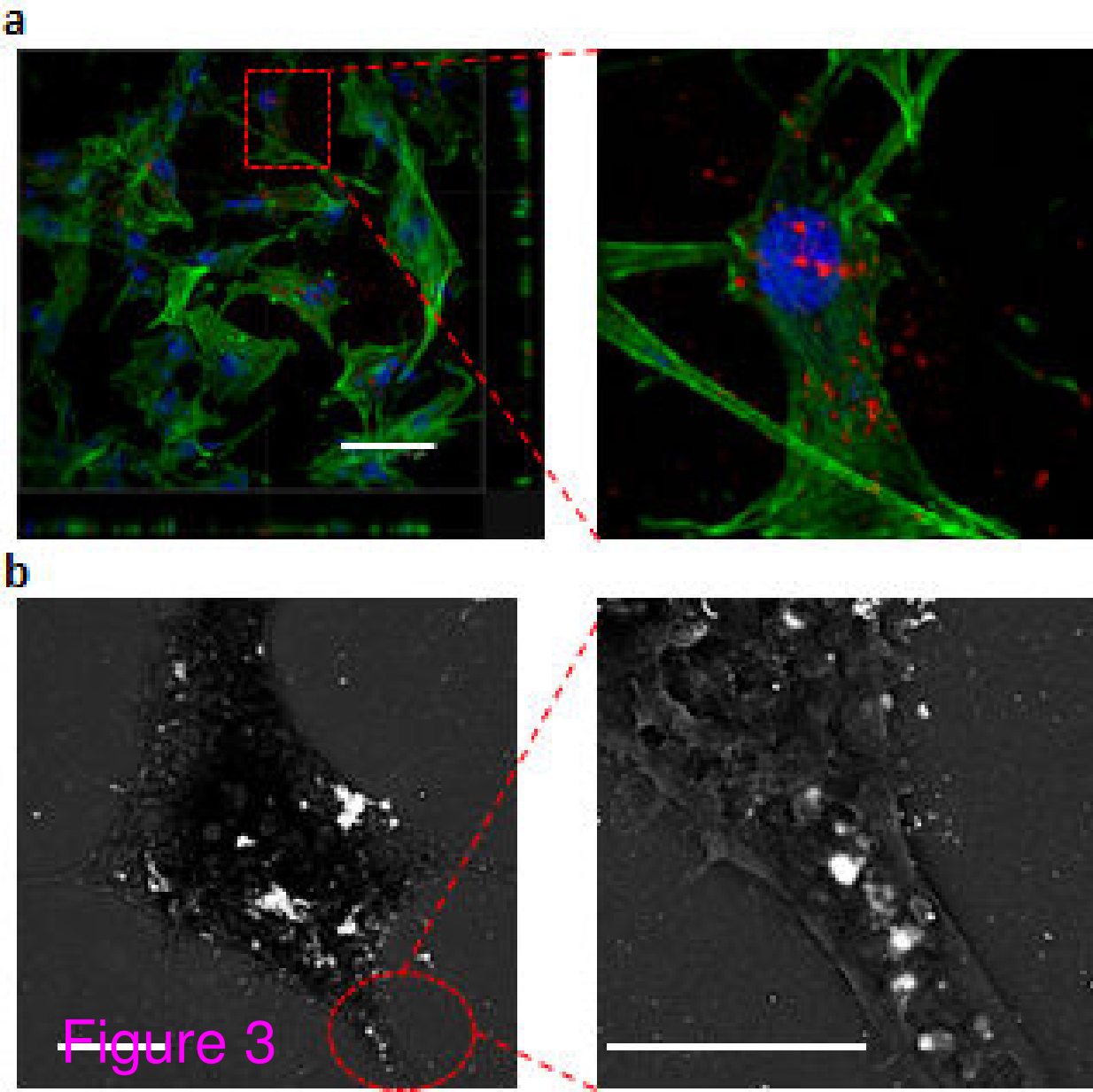
a
b
Figure 3

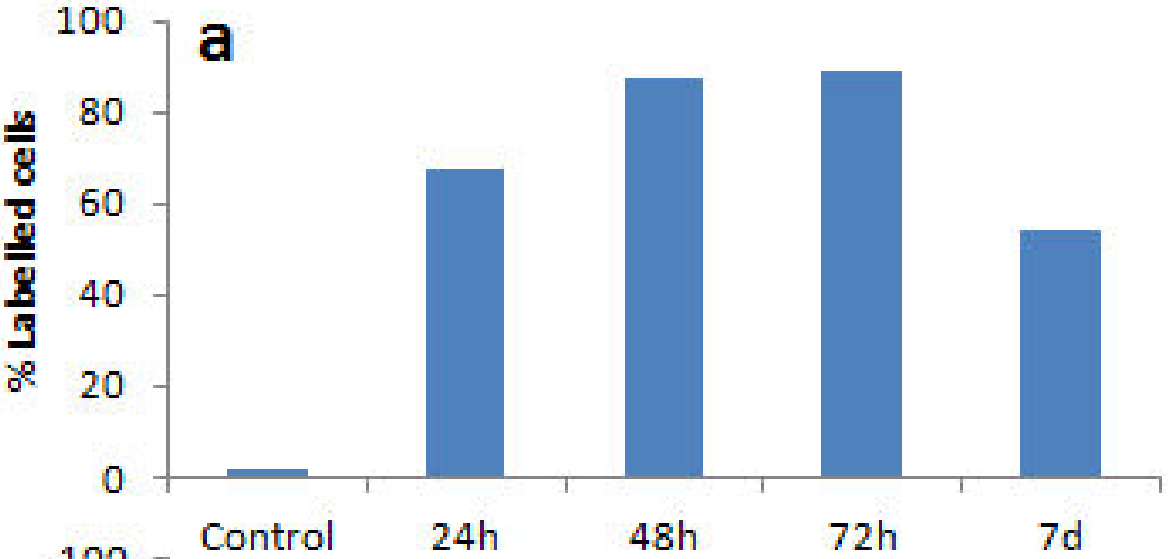
a
100
80
60
40
20
0
% Labelled cells
Control
24h
48h
72h
7d
Time

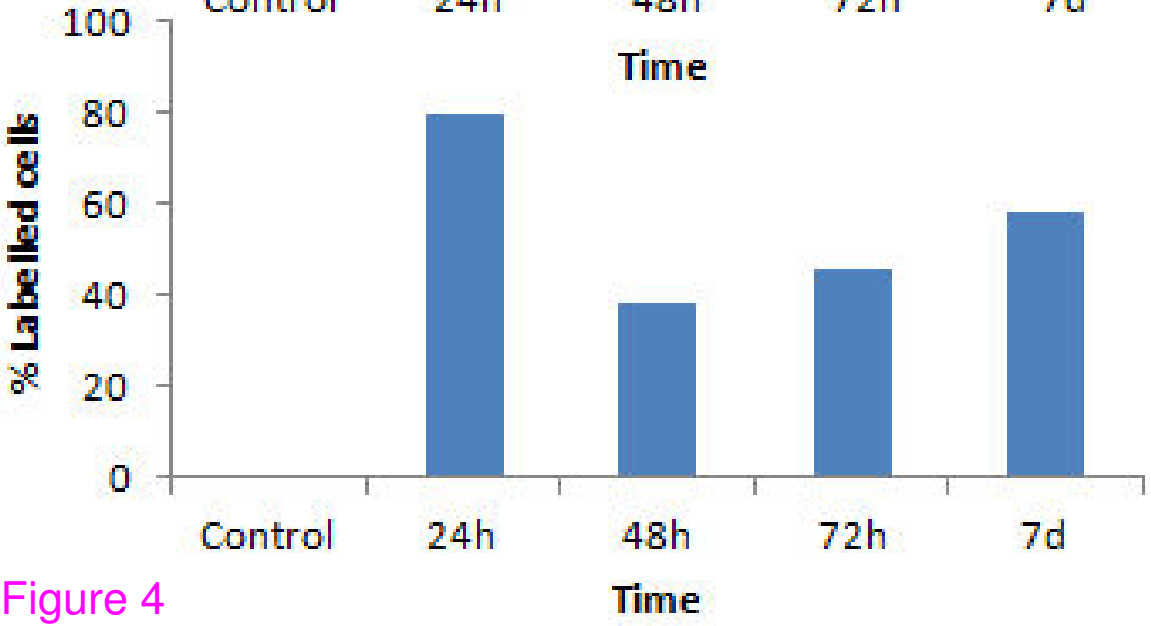
100
80
60
40
20
0
% Labelled cells
Control
24h
48h
72h
7d
Time

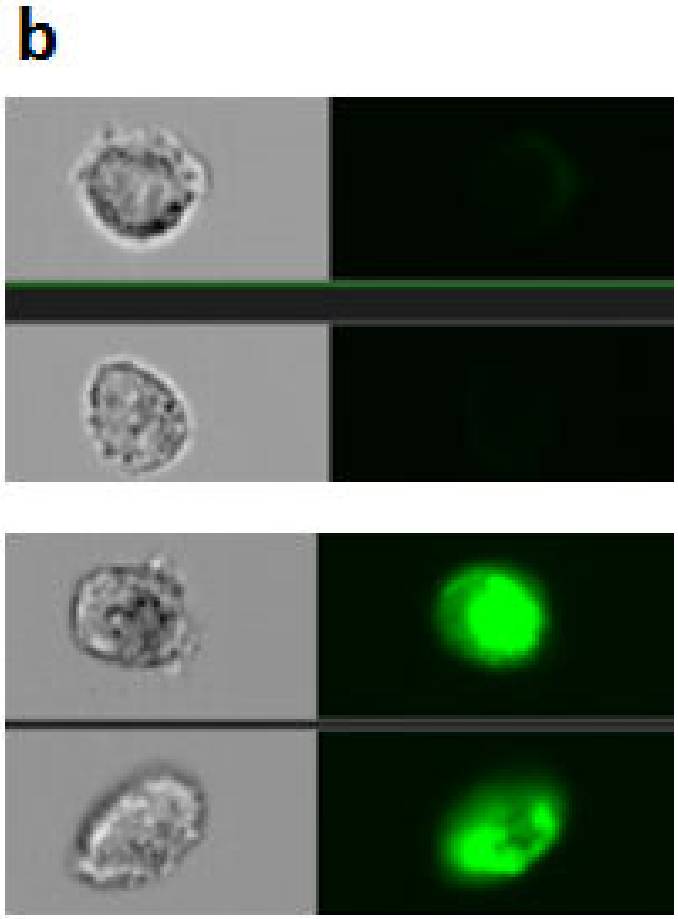
b

Figure 4

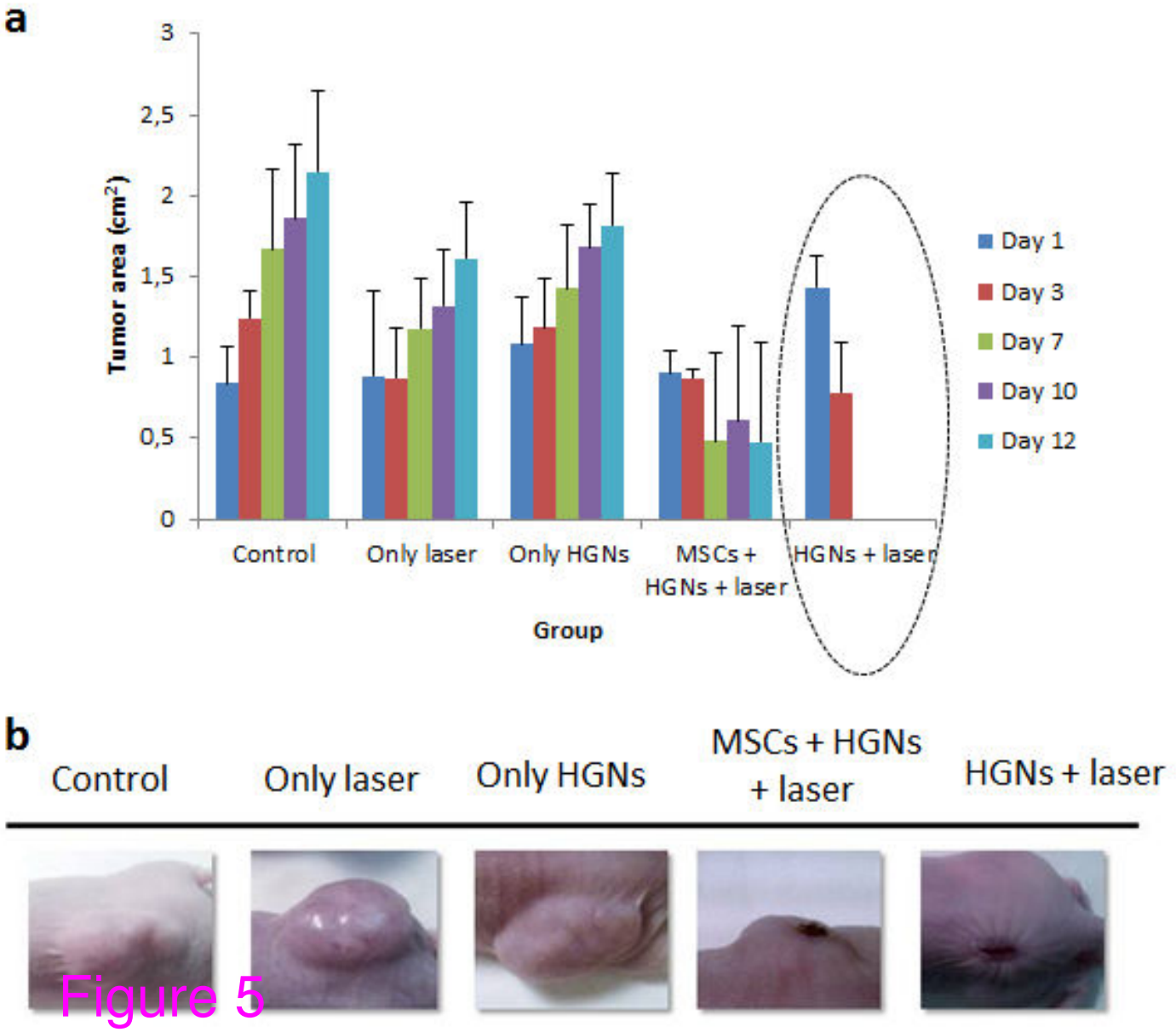
a
Tumor area (cm²)
3
2,5
2
1,5
1
0,5
0
Control
Only laser
Only HGNs
MSCs + HGNs + laser
HGNs + laser
Group
Day 1
Day 3
Day 7
Day 10
Day 12
b
Control
Only laser
Only HGNs
MSCs + HGNs + laser
HGNs + laser

Figure 5

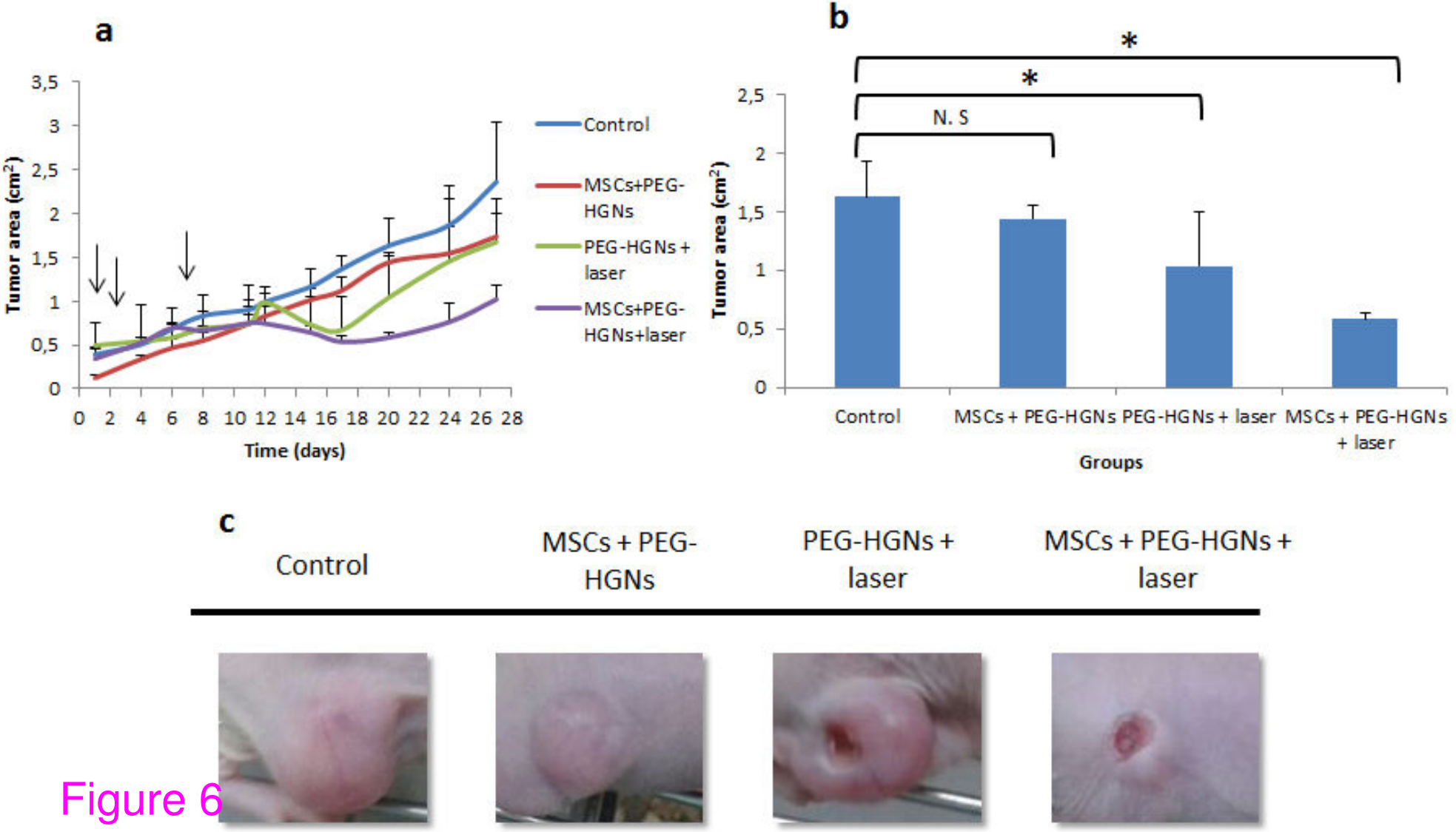
a
Tumor area (cm²)
Time (days)
Control
MSCs+PEG-HGNs
PEG-HGNs + laser
MSCs+PEG-HGNs+laser
b
Tumor area (cm²)
N. S
*
*
Control
MSCs + PEG-HGNs
PEG-HGNs + laser
MSCs + PEG-HGNs + laser
Groups
c
Control
MSCs + PEG-HGNs
PEG-HGNs + laser
MSCs + PEG-HGNs + laser

Figure 6

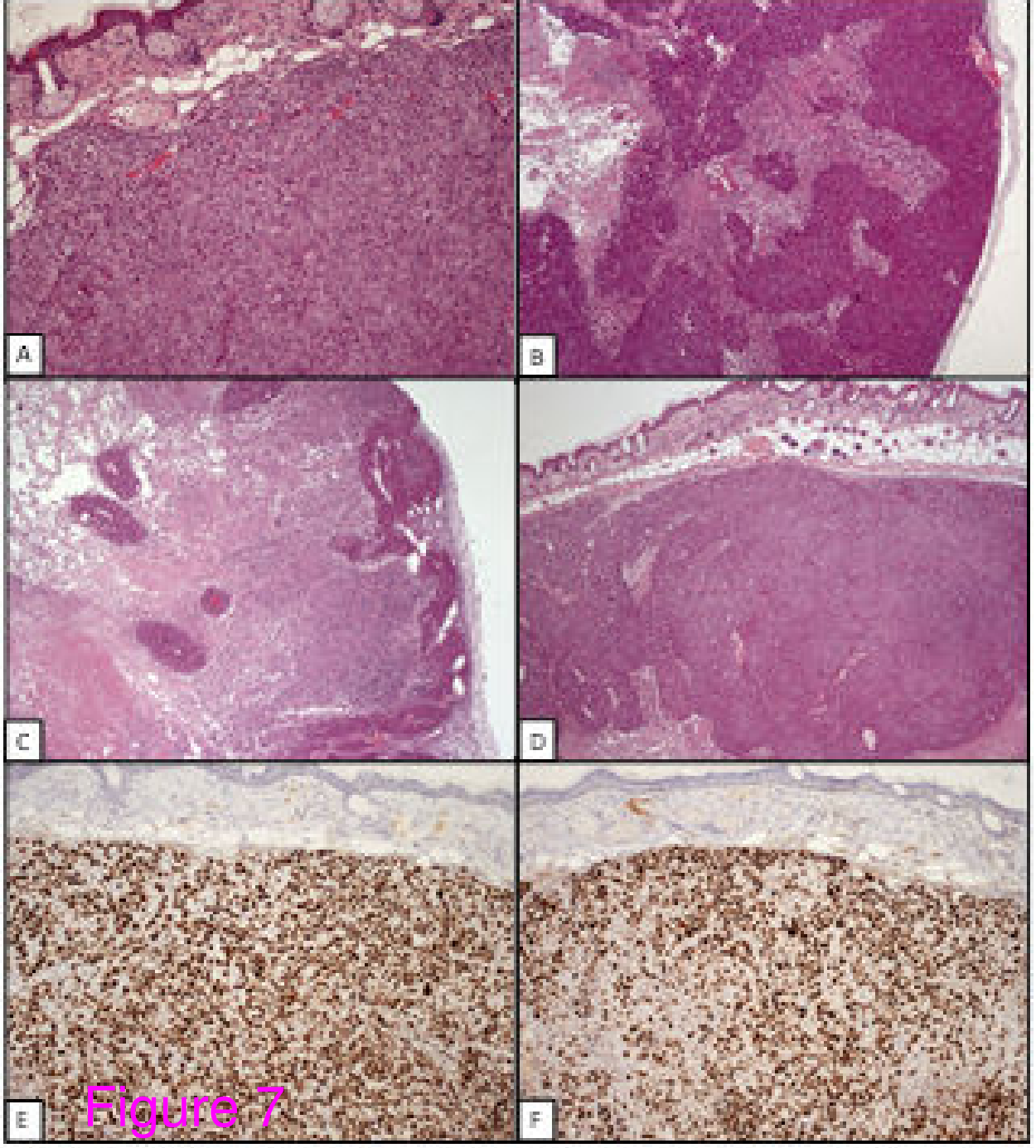

Figure 7

Additional files provided with this submission:

Additional file 1: SUPPORTING INFORMATION.pdf, 295K
http://www.biomedcentral.com/imedia/4709566821594200/supp1.pdf